3D Numerical Modeling of Circulations Associated with Submerged Buoyant Jet in a Shallow Coastal Environment

J. Jiang[a], D. B. Fissel[a] and D. Topham[b]

[a]*ASL Environmental Sciences Inc., 1986 Mills Rd., Sidney, BC, V8L 5Y3, Canada, jjiang@aslenv.com and dfissel@aslenv.com*
[b]*Topham Scientific Consulting Services Inc., 1925 Taylor Street, Victoria, BC, V8R 3G5, Canada, dtopham@islandnet.com*

Abstract: A three-dimensional numerical model was applied to examine the buoyant jet-driven circulation in Port Moody Arm, Canada. The Arm, which has a relatively shallow water environment of 5 – 30 m depth, receives considerable cooling water from Burrard Thermal Generating Station. The cooling water behaves as a typical submerged buoyant jet and has significant impact on the natural circulation of the receiving water. In order to resolve the sharp gradients in hydrothermal field and overcome the scale barrier between the far-field and near-field zones of the submerged buoyant jet, a newly developed embedded grid scheme was incorporated into the model, which solves the complete field with a single modeling procedure using a pre-conditioned conjugate gradient approach. Special care was taken with the turbulence diffusion and jet entrainment by using a second order turbulence closure model and the Smagorinsky formula. The simulated buoyant jet was calibrated using an integral model matched to empirical jet data; modeled velocity and temperature profiles were quantitatively verified as being in good agreement with the available observations. After the modeled flow pattern was qualitatively verified with data from historical dye-tracing surveys, extensive simulations were carried out to examine circulation behavior under the impact of the buoyant jet.

Keywords: Buoyant jet, circulation, embedded grid, 3D numerical model, temperature

Estuarine Coastal and Shelf Science, Volume 58, Issue 3, Pages 475 – 486

Introduction

Problem background

In building thermal or nuclear power stations at coastal regions, the removal of the waste heat is a major environment concern involving potential effects on the biotic system, especially fish and shellfish. The heated water discharged from these power plants is usually ejected into shallow waters as submerged buoyant jets (Sobey, *et al*., 1988), and results in changes to the natural circulation of the receiving waters. Consequently, the receiving waters are characterized by two different zones, so called near-field and far-field, which have different spatial scales, of the order of 100 m in the near-field zone and 1000 m in the far-field zone (GESAMP, 1984). Investigating the overall behavior of the buoyant jet and its associated circulation patterns are thus important to our overall understanding of the waste heat removing processes.

In many cases of interest, the receiving water body is density stratified in the vertical, and it is important that the characteristics of a concentrated heat source injected into the lower levels of the near field be correctly represented as a forcing function for the far field, which is often the primary interest of the study. The near-field zone features strong buoyancy plumes as well as intensive levels of entrainment, whereas the far-field zone has diluted plumes and associated mesoscale circulations. For input to the far-field it is necessary to define the point of impingement of the heated buoyant jet on the surface, together with the associated temperature and velocity distributions. If these near surface conditions can be accurately simulated, the detailed structure of the rising plume is not critical to the study.

Buoyancy plume mechanics in the near and complete field has been the subject of considerable researches over the past three decades. Previous studies of buoyancy plumes in the near-field were usually conducted through physical models (e.g., Sobey, *et al*., 1988; Johnston, *et al*., 1994), integral numerical models (e.g., Bemporad, 1994; Johnston, *et al*., 1994) or three-dimensional numerical models (e.g., Stolzenbach and Harleman, 1973; McGuirk and Rodi, 1979; Lavelle, 1997). These results have led to improved understanding of the buoyancy processes, and meanwhile, increased the capabilities of numerically modeling the receiving water circulation and thermal processes in the complete field. The mathematical plume models for the complete field are either of phenomenological (Dunn, *et al*., 1975; Jirka, *et al*., 1975) or three-dimensional numerical types, but fully three-dimensional numerical models are more applicable in engineering problems. In the latter approach, coupled hydrothermal equations are solved simultaneously in the complete field and fewer assumptions on the natural processes of the buoyant jet and ambient water have to be made. For example, Raithby *et al*. (1988) described a three-dimensional model for heated surface jets into quiescent lakes using an orthogonal boundary-conforming mesh to concentrate the model grids in the vicinity of the cooling water discharge and a k - ε model to calculate turbulent stresses and fluxes. GESAMP (1984) reported an alternative approach to model the complete zone in that the far-field and near-field zones were modeled separately and variables were interpolated back and forth between the coarse and fine meshes of these two zones. But so far, few have been presented on the simultaneous simulation and prediction of temperature and velocity field in complete receiving water with a submerged buoyant jet in place. Such a

simulation remains a hard task in part due to sharp gradients in the hydrothermal field, scale barrier and interface-coupling difficulties.

In the recent study of the Burrard Generating Station cooling water recirculation by the authors of this paper (Jiang, *et al*., 2001), substantial efforts were devoted to overcoming the above problems. The entire domain of the receiving waters in the Port Moody Arm was successfully simulated in a single modeling procedure using the 3D model ASL-COCIRM. A newly developed embedded grid and interface-coupling scheme was adapted in order to incorporate the essential features of both the submerged buoyant jet and the cooling water intake into the model. This paper will describe the key aspects of this study and present the simulated results of the circulations associated with the buoyant jet discharge to the receiving waters.

Brief description of study area

The Burrard Generating Station (BGS) is located on the north shore of the Port Moody Arm (hereafter, simply called the Arm), British Columbia, Canada (Figure 1). The Arm has a length of 6.5 km, a mean width of 0.9 km, and the mean water depth varies from 5 to 30 m. A mixed tide occurs with a mean tidal range of 3 m. Tidal currents are typically 10 – 20 cm/s or less. The BGS releases a large volume of heated cooling water (CW) into the Arm, with a maximum allowable discharge of 1.7×10^6 m^3/d at a maximum temperature of 27 ºC, which exceeds the temperature of the ambient water by about 4 – 10 ºC in summer and up to 20 ºC in winter. This cooling water discharge is released into the Arm through two independent outlet systems, each consisting of a pair of adjacent horizontal pipes, respectively denoted the shore side and sea side pipes, and takes the form of a submerged horizontal heated buoyant jet in a relatively shallow water depth of

approximately 10 m (Figure 1). The two shore side pipes are set at 3 m above the seabed with an outlet velocity U_1 along the shore, and two sea side pipes at 6 m above the seabed with an easterly outlet velocity U_2 (Jiang, *et al*., 2002). The cooling water intake is positioned 30 m SSE of the outlet at a depth of about 11 m (Figure 1).

The results of earlier two-dimensional numerical model and field investigations have shown that the cooling water has a significant impact on the natural circulation and thermal regime of the receiving waters (Seaconsult, 1995; Fissel, *et al*., 1998; Taylor and Fissel, 1999). Moreover, Fissel, *et al*. (1998) and Taylor and Fissel (1999) have demonstrated the importance of tidal-driven exchange and mixing of the waters of Burrard Inlet in moderating the warming of the Arm due to the BGS by which the BGS heat into surface layer leaves the Arm on the ebb tide and cooler water enters the Arm at depth on flood tide. However, little has been learnt so far of the features of the thermal buoyant jet and its role in the three-dimensional circulation in the receiving water. Thus, this study is intended to achieve improved insights into these behaviors.

Model formulations and embedded grid scheme

Governing equations

The model solves fully three-dimensional, shallow water hydrodynamic and thermal conservation equations in a sigma-coordinate system (Blumberg and Mellor, 1987), where the pressure is simply assumed hydrostatic. A second order turbulence closure model, as described in Mellor and Yamada (1982), is applied to calculate the vertical momentum diffusion coefficient. The horizontal diffusion coefficients, A_x in the *x*-direction and A_y in the *y*-direction, are evaluated using Smagorinsky's formula (Smagorinsky, 1963) as follows

$$A_x = A_y = \frac{1}{2} C_A dx dy \sqrt{\left(\frac{\partial u}{\partial x}\right)^2 + \frac{1}{2}\left(\frac{\partial v}{\partial x} + \frac{\partial u}{\partial y}\right)^2 + \left(\frac{\partial v}{\partial y}\right)^2} \quad (1)$$

where C_A is an empirical coefficient, which will be determined from modeling tests in terms of jet entrainment, *dx* and *dy* respectively represent the spatial grid sizes in *x*- and *y*-directions, and *u* and *v* are the horizontal velocities in the *x*- and *y*-directions, respectively. The Nikuradse relationships were selected to specify the effective bottom roughness, z_0, with respect to turbulence strength.

Boundary conditions

The boundary conditions of zero surface momentum flux (no wind stress) and bottom shear stress, as expressed in terms of a quadratic law, are employed. At the open boundaries, the water surface elevations are specified from measurements. Under inflows, open boundary conditions of temperature and salinity are specified using observed data, while for outflows, the conventional Sommerfeld radiation condition is applied (Sommerfeld, 1949).

Initial conditions

The initial conditions for ASL-COCIRM model runs were as follows: (1) All velocities were set equal to zero, (2) water elevation at each grid point was generated through linear interpolation of the prescribed values at the open boundaries, (3) water temperature and salinity inside the domain were specified through linear interpolation of field data at sites UR, UA–UE along the channel center (Figure 1).

Solution techniques

The governing hydrodynamic and thermal conservation equations are solved by the semi-implicit finite difference method in a staggered grid, which discretizes the

convective and horizontal diffusive terms by an Eulerian-Lagrangian scheme (Casulli and Cattani, 1994), and the barotropic and vertical diffusive terms by an implicit method. The modeled main-domain included the whole area of Port Moody Arm from the mouth at Burrard Inlet (Figure 1), and was resolved using a grid-size measuring 50 m × 50 m with 10 equally spaced vertical sigma-layers. Combining the differential continuity and momentum equations, a linear, five-diagonal system of equations for the water surface elevation, ζ, is obtained as the following generalized form

$$a_{i,j}\,\zeta_{i,j}^{n+1} - a_{i+1/2,j}\,\zeta_{i+1,j}^{n+1} - a_{i-1/2,j}\,\zeta_{i-1,j}^{n+1} - a_{i,j+1/2}\,\zeta_{i,j+1}^{n+1} - a_{i,j-1/2}\,\zeta_{i,j-1}^{n+1} = b_{i,j} \qquad (2)$$

where a and b are the coefficients dependent on hydrodynamic properties at time step n, the subscripts i and j denote the horizontal location indices and the superscript n represents the time step. This system is solved effectively by the pre-conditioned conjugate gradient method (Casulli and Cheng, 1992) along with the sub-domain in a single modeling procedure.

Embedded grid scheme

In the presence of a submerged buoyant jet, a much finer mesh in the near-field zone is required in order to resolve the sharp gradients in the hydrothermal field near the hydraulic jet. In the present study, in which the main interest is in the large scale circulation pattern in the presence of the cooling water flow, the primary purpose of the fine scale grid is to correctly transfer the initial jet hydrothermal conditions to an appropriate set of inputs to the larger scale grid of the main circulation model. Therefore, it is essential that the model has sufficient grids in the near-field to adequately capture the overall behavior of the buoyant jet at every time step.

Such mesh configuration can be accomplished using either unstructured grid or structured multigrid methods. The unstructured-grid methods have shown impressive flexibility on grid refinement (Mavriplis, 1997), while existing structured multigrid methods have limitations on high grid refinement as required by a buoyant jet. To obtain the necessary resolution for a buoyant jet using the latter method, one has to apply an adaptive multistep grid scheme in the hydrothermal field for each grid that has to be calculated in sequence (Berger and Colella, 1989), or an independent multiblock method in that hydrothermal fields in the coarse and fine meshes are calculated separately and interpolated at the interfaces (GESAMP, 1984; Mavripli, 1992; Ramsey, *et al*., 1996). To overcome above drawbacks, a newly developed embedded grid scheme is applied in ASL-COCIRM, where the near-field zone of the cooling water buoyant jet, as well as the intake, is embedded within the far-field zone using an extremely high resolution model grid, and these two zones are coupled together at their interfaces. The coupled system of hydrothermal equations is then solved at the same time in the complete field. The sub-domain has the spatial grid sizes of $dx' = dx/L$ and $dy' = dy/L$, with dx and dy denoting the spatial grid sizes of the main-domain and L representing the sub-divided step. This approach removes the constraint in a structured mesh on grid refinement and can apply extremely high refinement at a single step. It therefore reduces the coupled interfaces, and at the same time, allows the sharp gradients in the hydrothermal field.

Inside the sub-domain, the differential continuity, momentum and thermal conservation equations are the same as in the main-domain. At the interfaces, a coupling scheme is applied in terms of mass, momentum and thermal conservation. To ensure momentum, heat and salinity conservation at the interface, the flux forms of the momentum and

thermal conservation equations are applied there. By considering mass conservation at the interfaces, the resulting continuity equations are related to both the sub-domain and the main-domain grid points. The generalized continuity equations at sub-domain interior grid points and interface grid points, as shown in Figure 2, are given in Eqs. (3) – (5), respectively. The differential continuity equations at other interfaces will have similar forms.

The interior grid point in the sub-domain

$$a'_{i',j'}\,\zeta'^{n+1}_{i',j'} - a'_{i'+1/2,j'}\,\zeta'^{n+1}_{i'+1,j'} - a'_{i'-1/2,j'}\,\zeta'^{n+1}_{i'-1,j'} - a'_{i',j'+1/2}\,\zeta'^{n+1}_{i',j'+1} - a'_{i',j'-1/2}\,\zeta'^{n+1}_{i',j'-1} = b'_{i',j'} \qquad (3)$$

The interface grid point at the sub-domain side (square point in Figure 2)

$$\begin{aligned}&\left(a'^{it}_{m,2} + \frac{2a'_{m+1/2,2}}{L+1}\right)\zeta'^{n+1}_{m,2} - a'_{m-1/2,2}\,\zeta'^{n+1}_{m-1,2} - a'_{m,2+1/2}\,\zeta'^{n+1}_{m,3} - a'_{m,2-1/2}\,\zeta'^{n+1}_{m,1} - \\ &\left(\frac{2a'_{m+1/2,2}}{L+1}\right)\left(\beta'_{m+1/2,2}\zeta^{n+1}_{i,j-1} + \beta''_{m+1/2,2}\zeta^{n+1}_{i,j} + \beta'''_{m+1/2,2}\zeta^{n+1}_{i,j+1}\right) = b''_{m,2}\end{aligned} \qquad (4)$$

The interface grid point at the main-domain side (diamond point in Figure 2)

$$\begin{aligned}&\left[a^{it}_{i,j} + \sum_{j'=1}^{L}\left(\beta''_{m+1/2,j'}\frac{2a'_{m+1/2,j'}}{L+1}\right)\right]\zeta^{n+1}_{i,j} - a_{i+1/2,j}\,\zeta^{n+1}_{i+1,j} - \sum_{j'=1}^{L}\left(\frac{2a'_{m+1/2,j'}}{L+1}\zeta'^{n+1}_{m,j'}\right) - \\ &\left[a_{i,j+1/2} - \sum_{j'=1}^{L}\left(\beta'''_{m+1/2,j'}\frac{2a'_{m+1/2,j'}}{L+1}\right)\right]\zeta^{n+1}_{i,j+1} - \left[a_{i,j-1/2} - \sum_{j'=1}^{L}\left(\beta'_{m+1/2,j'}\frac{2a'_{m+1/2,j'}}{L+1}\right)\right]\zeta^{n+1}_{i,j-1} = b''_{i,j}\end{aligned} \qquad (5)$$

where a' and b' are the coefficients derived from embedded grid, ζ' is the water surface elevation at the cell centers of the sub-domain, b'' is the combined coefficient of both the main and embedded grids at the interface, β is the weighting coefficient, with $\beta'+\beta''+\beta'''=1$, and a^{it} is a coefficient excluding the interface side, e.g., $a'^{it}_{m,2} = 1 + a'_{m-1/2,2} + a'_{m,2+1/2} + a'_{m,2-1/2}$ in Eq. (4) and $a^{it}_{i,j} = 1 + a_{i+1/2,j} + a_{i,j+1/2} + a_{i,j-1/2}$ in Eq. (5). Although the resulting differential continuity equations at the interface involve

more than 5 grid points, with 7 points at the sub-domain interface grid [Eq. (4)] and (4+*L*) points at the main-domain interface grid [Eq. (5)], the differential Equations (2) – (5) are combined into a positive-definite linear system, and therefore, have an unique solution. Thus, the combined linear system is solved by the pre-conditioned conjugate gradient method in all grid cells and every time step with a single modeling procedure.

The buoyant jet entrainment and diffusion are represented in the model by Smagorinsky's formulation and the second order turbulence closure model. As seen in Eq. (1), the Smagorinsky formula represents the horizontal diffusion as a function of velocity shear. After adjusting the Smagorinsky coefficient through model calibrations against an empirical relationship and integral solutions, the buoyant jet will be represented appropriately in the 3D model. In the turbulence closure sub-model, all empirical constants were assigned the values based on the laboratory data of Mellor and Yamada (1982).

In the present application, the embedded sub-domain covers an area of 300×200 m^2 (Figure 1) with *L*=20, which results in a horizontal resolution of 2.5 m × 2.5 m. It has the same vertical layers as the main-domain. Within the sub-domain, selected cells of the equivalent area are used to represent the outlet pipes, i.e., 4.67 m^2 for each individual pipe (Jiang, *et al.*, 2002). By specifying the jet discharge, exit temperature, salinity and mass concentration in these cells, the conservation of mass, thermal flux and total momentum over tidal cycles is then satisfied.

Model calibration and verification

Buoyant jet

An integral model of the buoyant jet was used as a standard of comparison, for the selection of appropriate vales of the Smagorinsky coefficient. The integral model solves the radially integrated conservation equations following the jet axis. The equations are similar to those introduced by Bemporad (1994), but with the drag coefficient associated with cross flows replaced by a modified application of the standard entrainment assumption. In the present application, the jet is injected horizontally and impacts the surface at a relatively shallow angle of around 10°. The argument is made that the horizontally injected vorticity dominates the entrainment, the vertical component of vorticity generated by the buoyancy being largely cancelled by the mixing across the centerline of the jet driven by the horizontal component. In this form, the entrainment is proportional to the horizontal component of the jet velocity difference.

$$\frac{dQ}{dS} = 2\pi\alpha_j R\left|u_t \cos\psi - u_\infty\right| \tag{6}$$

where Q is the jet flow rate, S is the distance along the trajectory, α_j is the dimensionless entrainment coefficient, R is the mean jet radius, u_t is the mean of the tangential jet velocity, ψ is the angle of the trajectory with horizontal axis, and u_∞ represents the local ambient velocity. With the entrainment constant α_j set at the standard value of 0.08 for the neutrally buoyant jet with Gaussian velocity profiles, empirical results for buoyant jets in both air and water are matched over a wide range of conditions.

The numerical model was calibrated for the simple case of a neutrally buoyant jet discharging into a stagnant homogenous environment. The neutral jet was set at 4 m

above bottom with an outlet velocity of 2 m/s. The empirical coefficient C_A in Eq. (1) was adjusted until the simulated entrainment rate realized a best fit with Eq. (6). The resulting steady flow was used to calculate the discharge Q at different cross-sections and consequently the entrainment rate, $\Delta Q / \Delta S$. The calibration results show that the model reproduced the entrainment rate of the neutrally buoyant jet reasonably well using the empirical values of C_A=0.3. The correlation coefficient, r, between modeled and empirical entrainment rates is found to be 0.89. This value of the Smagorinsky coefficient thus provides the correct matching of the mean temperature, buoyancy and velocity along the jet axis.

The model was then run with this coefficient for a buoyant jet discharging into a stagnant environment of typical summer stratification, with a cooling water discharge of 19.6 m^3/s, outlet velocity of U_2=2.0 m/s and outlet temperature of 26 °C. Figure 3 compares the numerical model outputs in the embedded grid area with the corresponding integral model results and field measurement. The temperature and velocity fields of the simulated buoyant plume are compared with the integral model results of the centerline velocities and centerline temperatures together with the observed temperature at BO (Figure 1), derived from the averaging of half hourly measurements over the same period. The trajectory and the centerline values are well reproduced, with the jet impinging on the surface about 30 m from the outlet, where it continues as a surface jet. At BO, the simulated temperature profile is in good agreement with observation. Therefore, the calibration of the diffusion coefficients based on the simple non-buoyant jet has faithfully reproduced the more complex behavior of the buoyant jet exiting into a stratified environment.

Vertical structures of velocity and temperature

In this study, extensive model experiments were conducted to validate the hydro- and thermo-models performance using observations to specify the open boundary and cooling water conditions. Quantitative comparisons between simulated and observed velocity and temperature profiles at the survey sites as shown in Figure 1 were then made. These comparisons included the hourly ADCP velocity profiles at site AD during the period of September 30 to October 27, 1998, Ekman current profiles at site WA during the period of January 26 – 27, 1962 (Waldichuk, 1965), and CTD temperature profiles at sites BT, BO, IN, PE, RP (Figure 1) during winter, summer and fall seasons, respectively. Detailed results of these comparisons were reported in Jiang *et al*. (2001, 2002). Overall, the modeled velocities and temperatures are found to be in very good agreement with the observations, with the correlation coefficients of modeled versus observed results up to 0.91 or better for currents and 0.95 or better for temperatures at most sites.

Flow pattern verification using dye tracing

The dye-tracing data from two historical surveys were used to verify the simulated flow patterns. These surveys were respectively conducted during ebb and flood tides under autumn conditions, with the cooling water discharge of 6.1 m^3/s and the outlet temperature of about 20.5 ^oC (Hodgins and Webb, 1991). At each survey, a total of 5.4 kg of rhodamine dye was pumped into the surge shaft in the generator hall over 3 – 4 hours. Dye concentration monitoring then started about one hour after the beginning of dye release using a ship-borne dye sensor. The dye sensor recorded the maximum dye concentration from 2 to 4.5 m depth as the survey vessel moved along the tracks shown

in Figure 4. It took about 3 hours for all the measurements in each individual survey to be accomplished.

In model simulations, the same amount dye, i.e., 5.4 kg, was released into the Arm and the model ran over the same period as the surveys. At the end of the simulation, the maximum dye concentration at 2 – 4.5 m depth was outputted and compared with the observations. Figure 4 shows the comparisons between observed and simulated dye dilution, D_e, where D_e is calculated in terms of $D_e = F_j / F$, with F denoting the maximum dye concentration at 2 – 4.5 m depth and F_j representing that within 10 to 15 m of the outlet pipe.

A direct comparison with the measurements is difficult, as these were not synoptic and the coverage is unevenly distributed. The ebb tide data consists of 12 irregular transects taken 3.3 hours, two outline the bottom of the lobed structures of the southern boundary (Figure 4); the region between these lobes containing little or no data. The flood tide data consists of 16 individual transects taken a period of 4.7 hours, giving reasonably even coverage over the whole plume (Hodgins and Webb, 1991). Given the nature of the survey, there is reasonable qualitative agreement with the overall plume shape derived from the measurements, with the exception of the area between the southern lobes of the ebb tide plume (Figure 4). This area of the survey is one of extremely spare coverage, and there may be considerable doubt as to the placing of the contours.

Circulations associated with the buoyant jet

The typical natural circulations inside the Arm (Jiang, *et al*., 2001) show that the effect of temperature and salinity induced stratification is only evident near the mouth of the Arm, where the modeled results reveal a down-inlet residual near the surface and an up-

inlet residual near the south shore at all levels, with the magnitude less than 2 – 3 cm/s. In remaining areas, the residuals seem to be mainly caused by local irregular geometry with a magnitude generally less than 2 cm/s. In the narrow section, a counter-clockwise eddy occupies all levels. Further up-inlet, a counter-clockwise eddy appears at the north shore side, whereas a clockwise eddy appears at the south shore side.

Under winter conditions, for a low cooling water discharge of Q_{CW} =4.9 m^3/s, a weak outlet velocity of U_2 =0.5 m/s, and a cooling water temperature of T_{CW} =23 °C, the model results (Figure 5) show that the submerged buoyant jet rises to the surface at about 20 m from the outlet. After surfacing, most of the warmer water propagates forward in the format of a surface buoyant jet, which has strength of 10 – 15 cm/s at the near-field zone and becomes weaker, reduced to as low as 2 – 5 cm/s, as it propagates up-inlet. As the discharged water gradually turns down-inlet following the geometry of the Arm, it results in a pronounced down-inlet residual at near-surface layer, with the magnitude ranging from 4 to 6 cm/s. In addition, a considerable part of the warmer water reverses after surfacing and flows along the west side of the outlet and intake before it joins the main surface flow at southwest corner (Figure 5). This feature replicates the reverse flow at low densimetric Froude number from the theoretical results of Johnston, *et al*. (1994). At the mid-depth, an up-inlet residual appears in the middle channel where water depths typically exceed 15 – 20 m, and part of the residual discharge is then entrained into the jet. The typical strength of the residual at this level is 2 – 4 cm/s. The near-bottom level is also dominated by an up-inlet residual, with significant part of it taken into the intake and the buoyant jet (Figure 5). The strength of residual near the bottom is close to those of the middle depth. The modeled residual currents also exhibit uneven cross-sectional

distributions around the narrow section. At the relatively shallow areas near the shores, with water depth typically less than 10 – 20 m, the residual currents seem to follow the same patterns as the natural circulations and the down-inlet residuals dominate the entire water column, while in the middle channel, up-inlet residuals dominate the deeper levels.

The simulated thermal plume from the cooling water is accordingly confined to the near-surface layer, and evidently follows the circulation patterns (Figure 5). The near-surface tidally-averaged water temperatures are about 13 °C in the near-field zone, and 9 – 11 °C in most of the far-field zone, increasing by 1 – 3 °C if compared with the ambient water temperature (T_{AW}) which was taken as the vertically-averaged inflow water temperatures measured at UR. At the mid-depth and near-bottom, tidally-averaged water temperatures are 7.8 – 8.5 °C, very close to those without the BGS in operation. In other words, little heat is mixed down to these deeper layers, and at the same time, significant inflow of colder water from adjoining ocean occurs there because of the up-inlet residuals.

As the cooling water discharge increases, one can expect a more significant impact on the natural circulation of the receiving water. Figure 6 shows the modeled results for autumn conditions under a high cooling water discharge of 19.6 m^3/s. It has a cooling water outlet temperature of 26 °C, the sea side outlet velocity of U_2=1.5 m/s, and shore side outlet velocity of U_1=0.5 m/s. The vertically-averaged ambient water temperature, T_{AW}, is equal to 11.2 °C, and the mean ambient near-surface temperature is about 11.7 °C. The model yields very similar residual patterns to those described for the winter with a low Q_{CW}. However, some differences are observed. The residual flows generally

increases by 1 – 3 cm/s in magnitude at all levels, when compared with the low Q_{CW} case. The submerged buoyant jet rises to the surface within 20 – 30 m of the cooling water outlet, with the shore side jet surfacing at a closer distance (not shown), being in good agreement with field observations (Jiang, *et al.*, 2001). Before turning down-inlet, the surface buoyant jet propagates much further up-inlet than the low Q_{CW} case. The core velocities of the surface buoyant jet are 10 – 40 cm/s. Instead of considerable reverse flow at the backward area of the surface jet, there is evidence of entrainment into it and consequently a small clockwise eddy develops to the southeast outlet and intake structure, because of a higher densimetric Froude number.

Again, the thermal plume from the cooling water discharge is only found at the near-surface layer. It obviously follows the circulation patterns as stated above and extends over a much larger area than the low Q_{CW} case (Figure 6). The near-surface water temperatures are about 17 °C in the near-field zone, and 13 – 16 °C in most of the far-field zone, an increase of 1 – 5 °C compared with the ambient water temperature. At the mid-depth and near-bottom, tidally-averaged water temperatures are 11.2 – 12.5 °C, very close to those without the BGS in operation. Once again, it suggests that little heat is mixed down to these layers, and meanwhile, there is significant inflow of colder water from the adjoining ocean associated with the up-inlet residuals.

Around the narrow section, the modeled residual currents exhibit a similar uneven cross-sectional distribution to the low Q_{CW} case, with the strength slightly increased. Figure 7 shows vertical profiles of the residual currents respectively at the site WA (middle channel with a mean depth of 22 m, see Figure 1), site AD (middle channel with a mean depth of 30 m), and site NS (near north shore with a mean depth of 19 m).

Comparisons to the observations are also included at WA and AD, while no observations are available at NS. It is seen that at WA and AD, the simulated residuals are in reasonable agreement with the observations. Both simulations and observations show that the down-inlet residuals appear to occupy a relatively thin near-surface layer, about 5 – 10 m from the surface, whereas the up-inlet residuals dominate the deeper levels. Therefore, a net up-inlet mass flux is expected in the middle channel. At NS, the down-inlet residual dominates the entire water column except for a very thin near-bottom layer (Figure 7), and consequently results in a net down-inlet mass flux. Figure 7 also shows that residual currents increase with the increase in the cooling water discharge.

Presented above are the representative results of numerous model runs conducted in this study. Other modeled results exhibit similar circulation patterns, and thus, are not presented here. Overall, the model predicted very reasonable circulation patterns associated with the submerged buoyant jet in the receiving water. The buoyant jet rises to the surface within 20 – 30 m from the cooling water outlet, which is in good agreement with observations. Very strong local entrainment of ambient water is involved during its rising stage. Afterward, it propagates forward in the form of a surface buoyant jet. At the same time, the buoyant jet follows the geometry of the Arm and gradually turns down-inlet, and consequently results in the near-surface down-inlet residual flow in most areas of the Arm at near surface levels. At a relatively low exit velocity, a considerable part of the cooling water turns backward, which consistently replicates the reverse flow theory of Johnston, *et al*. (1994) under a low densimetric Froude number. At the middle channel, the up-inlet residuals dominate all the deeper levels, and exhibit the same vertical structures as the observations, e.g., sites WA and AD. At the relatively shallow area near

the shores, the simulated residual currents under the influence of the cooling water discharge appear to follow similar patterns to the natural circulations and down-inlet residuals dominate the entire water column. Although no observations are available for comparisons in those areas, one can phenomenologically conclude such residual features from the fact that in terms of mass conservation, the net up-inlet mass flux in the middle channel leads to a net down-inlet mass flux in the form of a dominant down-inlet residual flow in near-shore areas.

Conclusion and discussion

In this study, the 3D numerical model ASL-COCIRM was applied to a tidal inlet containing a concentrated input of heated water from a generating station. A sub-domain was calibrated to simulate the buoyant jet entrainment, trajectory, centerline dilution, temperature and velocity profiles, and nearby flow patterns. Although the large scale simulated flow patterns could only be qualitatively verified from historical dye-tracing data, the results demonstrate that the model has the capability of predicting the receiving water circulations under the influence of a submerged buoyant jet in shallow receiving waters. The model provides a useful tool for studying buoyant jet associated mesoscale circulations in the receiving water, waste heat removing processes and cooling water recirculation to the intake (Jiang, *et al*., 2001).

In the present application to Port Moody Arm, the predicted vertical structures of the residuals at the survey stations WA and AD are in reasonable agreement with the observations. Overall, the BGS cooling water discharges generate a down-inlet near-surface residual, and an up-inlet residual which dominates the deeper layers in the middle channel. Such a circulation pattern is consistent with a high level of heat exchange

between waters of the Arm and the adjoining ocean, as modulated by the tidal forcing. As a consequence, the warmer cooling water is flushed out of the Arm through the upper layer, about 5 – 10 m depth from the surface, while colder water from the adjoining ocean intrudes into the Arm from the deeper layers, usually below 5 – 10 m depth. This deepwater inflow is then entrained into the cooling water intake as well as the buoyant jet. These results replicate the previous empirical conclusions derived from extensive analysis of the field observations (Taylor and Fissel, 1999; Birtwell, *et al*., 2001).

The complete linear system of water surface elevation in the entire modeled domain [Eqs. (2) – (5)] was implicitly solved by pre-conditioned conjugate gradient method. Such an algorithm allows the use of a large sub-divided step, *L*, to provide high resolution in the sub-domain. The present embedded grid model has a resolution of 2.5 m by 2.5 m, compared with 50 m by 50 m in the main-domain. It represents the processes of the submerged buoyancy plume and the structure of outlet pipes and intake in a realistic manner. The buoyant jet turbulence diffusion and entrainment are included through the second order turbulence closure model and the Smagorinsky formula in the model. The modeled buoyant jets are in good agreement with empirical relationships, an integral model, and field measurements, in terms of the jet entrainment, trajectory, dilution and surfacing location. The value of the Smagorinsky coefficient required to match the model performance to known jet properties is retained throughout the entire model, on the grounds that the influence form this diffusion term becomes of minor importance over the larger domain.

The universally applicable approach was adopted in order to deal with the complex time dependent physical processes in the complete near and far field of a submerged

buoyant jet. Such approaches can avoid inconsistencies between the sub-domain and the main-domain as well as in the vertical, and reduce the problems which arise from a separate integral model for the jet. Similar methods have been successfully applied to model the complete field as a heated surface jet in place (e.g., Raithby, *et al*., 1988). However, the present performance of this method is only based on the preliminary model tests. Further studies are necessary to investigate the universally applicable approaches for the physical processes in the complete field with a submerged buoyant jet in place.

Acknowledgements

We thank the Burrard Thermal Generating Station, BC Hydro, for the opportunity to undertake this study, in particular Mr. Al Brotherston who supervised the project of Burrard Generating Station Cooling Water Recirculation Study. Our thanks also extend to Dr. R. Thomson of the Institute of Ocean Sciences, and Dr. J. W. Lavelle of Pacific Marine Environmental Laboratory, NOAA, for their valuable suggestions and discussions on how to incorporate a submerged buoyant jet into 3D numerical model. Several other personnel at ASL, in particular David Lemon and Alan Taylor, assisted in model development and data collection. Mike Henry of the University of British Columbia made his monthly water temperature and salinity profile measurements available to this study.

References

Bemporad, G. A. 1994 Simulation of round buoyant jet in stratified flowing environment. *Journal of Hydraulic Engineering*, ASCE, 120, 529-543.

Berger, M. J. & Colella, P. 1989 Local adaptive mesh refinement for shock hydrodynamics. *J. Comp. Phys*., 82, 64-84.

Birtwell, K. L., Brotherston, A. E., Fink, R. P., Fissel, D. B., Greenbank, J. D., Heithaus, L. I., Korstrom, J. S. & Taylor, A. E. 2001 Thermal Inputs into Port Moody Arm, Burrard Inlet, BC, and Effects on Salmon: a Summary Report. *Canadian Technical Report of Fisheries and Aquatic Sciences 2340*, p35.

Blumberg, A. F. & Mellor, G. L. 1987 A description of a three-dimensional coastal ocean circulation model. In: *Three-Dimensional Coastal Ocean Models*, N. S. Heaps ed., American Geophysical Union, Washington, DC, 1-16.

Casulli, V. & Cattani, E. 1994 Stability, Accuracy and Efficiency of a semi-implicit method for three-dimensional shallow water flow. *Computers Math. Applic.*, 27, 99-112.

Casulli, V. & Cheng, R. T. 1992 Semi-implicit finite-difference method for three-dimensional shallow water flow. *International Journal for Numerical Methods in Fluids*, 15, 629-648.

Dunn, W. E., Policastro, A. J. & Paddock, R. A. 1975 Surface thermal plumes: Evaluation of mathematical models for the near and complete field. *Argonne Natl. Lab. Report ANL. WR-75-3*, Argonne, p11.

Fissel, D. B., MacNeil, M. & Taylor, A. E. 1998 A Study of the Thermal Regime of Port Moody Arm in Relation to the Burrard Thermal Generating Station. *ASL Report: 41-377-F*, ASL Environmental Science Inc., Sidney, BC, Canada, p64.

GESAMP, 1984 Thermal Discharges in the Marine Environment. *Reports and Studies No. 24*, Food and Agriculture Organization of the United Nations, p44

Hodgins, D. O. & Webb, A. J. 1991 Determination of Residual Chlorine in Burrard Inlet Originating from the Burrard Thermal Generating Plant. Seaconsult Marine Research Ltd., Vancouver, BC, p55.

Jiang, J., Fissel, D. B., Lemon, D. D. & Topham, D. 2002 Modeling cooling water discharges from the Burrard Generating Station, BC Canada. *Proceedings of Oceans 2002 MTS/IEEE*, Biloxi, Mississippi, October, 2002 (in press).

Jiang, J., Fissel, D. B. & Taylor, A. E. 2001 Burrard Generating Station Cooling Water Recirculation Study. *ASL Report: 41-452-f*, ASL Environmental Sciences Inc., Sidney, BC, Canada, p45.

Jirka, G. H., Abraham, G. & Harleman, D. R. F. 1975 An assessment of techniques for hydrothermal prediction. *Report 203*, Ralph M. Parson Lab. For Water Resource and Hydrodynamics, Massachusetts Institute of Technology, Cambridge, Mass.

Johnston, A. J., Phillips, C. R. & Volker, R. E. 1994 Modeling horizontal round buoyant jets in shallow water. *Journal of Hydraulic Engineering*, 120, 41-59.

Lavelle, J. W. 1997 Buoyancy-driven plumes in rotating, stratified cross flows: plume dependence on rotation, turbulent mixing and cross-flow strength. *Journal of Geophysical Research*, 102, 3405-3420.

Mavriplis, D. J. 1992 Three-dimensional multigrid for the Euler equations. *AIAA J.* 30, 1753-1761.

Mavriplis, D. J. 1997 Unstructured grid techniques. *Annual Review of Fluid Mechanics*, 29, 473-514.

McGuirk, J. J. & Rodi, W. 1979 Mathematical modelling of three-dimensional heated surface jets. *Journal of Fluid Mechanics*, 95, 609-633.

Mellor, G. L. & Yamada, T. 1982 Development of a turbulence closure model for geographical fluid problems. *Review of Geophysics*, 20, 851-875.

Raithby, G. D., Elliott, R. V. & Hutchinson, B. R. 1988 Prediction of three-dimensional thermal discharge flows. *Journal of Hydraulic Engineering*, 114, 720-737.

Ramsey, J. S., Hamilton, R. P. & Aubrey, D. G. 1996 Nested three-dimensional hydrodynamic modeling of the Delaware Estuary. In: *Proceedings of the 4th International Conference on the Estuarine and Coastal Modeling*, ASCE Waterway, Port Coastal and Ocean Division, 53-65.

Seaconsult, 1995 Receiving water impact assessment for Burrard Thermal Generating Plant. Prepared for BC Hydro, Burnaby, BC, p58.

Smagorinsky, J. 1963 General circulation experiments with the primitive equations: I. The basic experiment. *Monthly Weather Review*, 91, 99-164.

Sobey, R. J., Johnston, A. J. & Kreane, R. D. 1988 Horizontal round buoyant jet in shallow water. *Journal of Hydraulic Engineering*, 114, 910-929.

Sommerfeld, A. 1949 Partial differential equations. *Lectures in Theoretical Physics*, 6, Academic Press.

Stolzenbach, K. D. & Harleman, D. R. F. 1973 Three-dimensional heated surface jets. *Water Resources Research*, 9, 123-137.

Taylor, A. E. & Fissel, D. B. 1999 A study of the thermal regime of Port Moody Arm, Volume I. *ASL Report: 41-399-F*, ASL Environmental Sciences, Sidney, BC, Canada, p50.

Waldichuk, M. 1965 Water exchange in port Moody, British Columbia, and its effect on waste disposal. *Journal of Fisheries Research Board of Canada*, 22, 801-822.

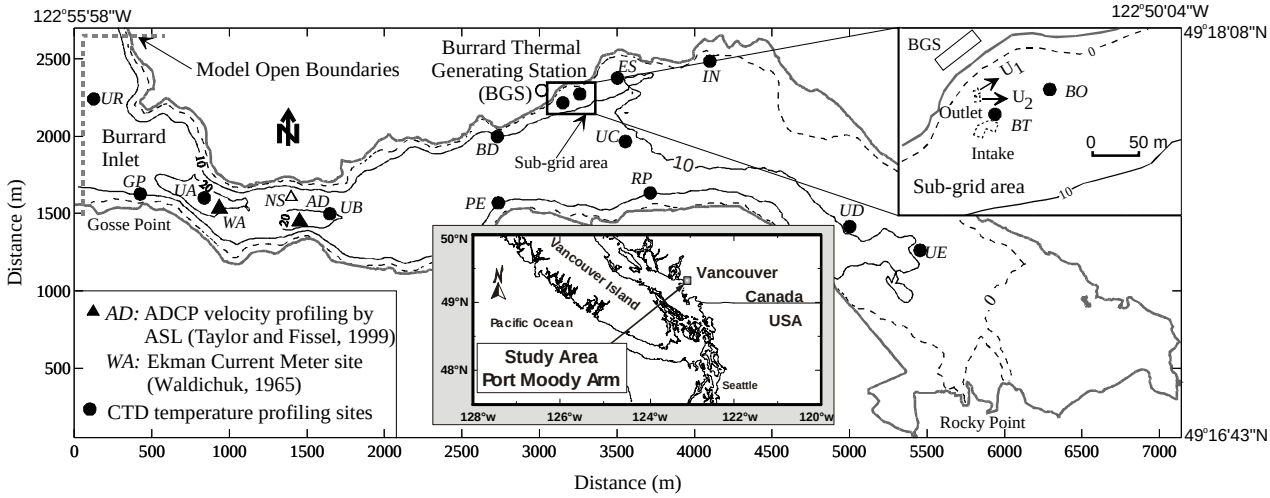

FIGURE 1. Location map of the Port Moody Arm, cooling water outlet and intake, and survey sites of temperature and currents. Depths are in meters below lowest astronomical tide.

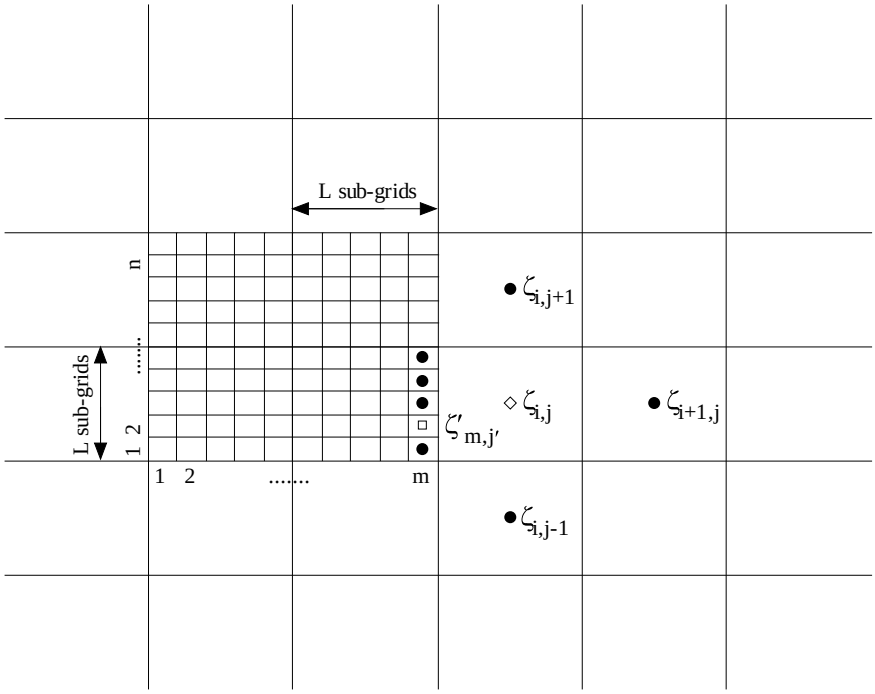

FIGURE 2. Schematic diagram showing embedded grid.

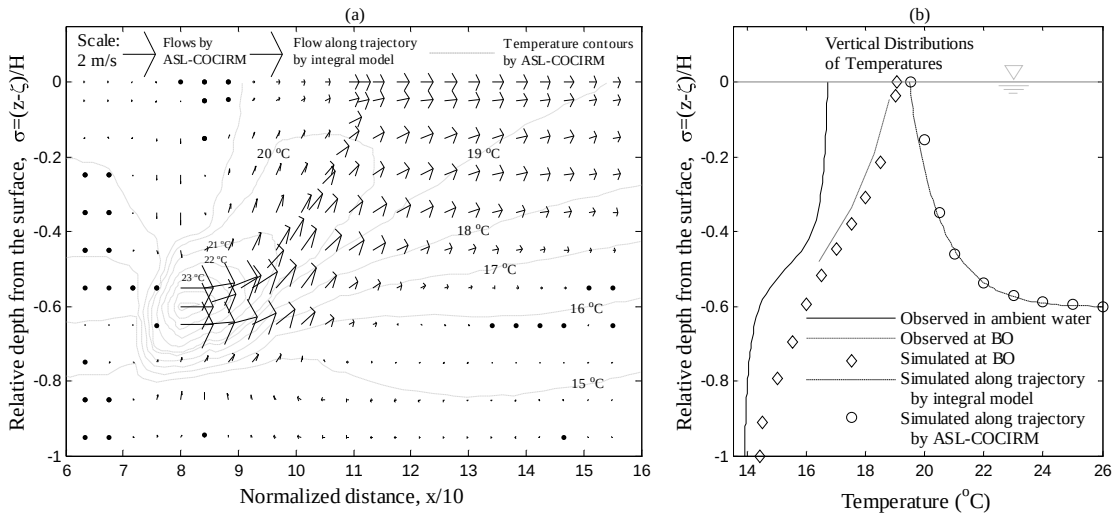

FIGURE 3. Buoyant jet (a) and vertical structures of temperatures (b).

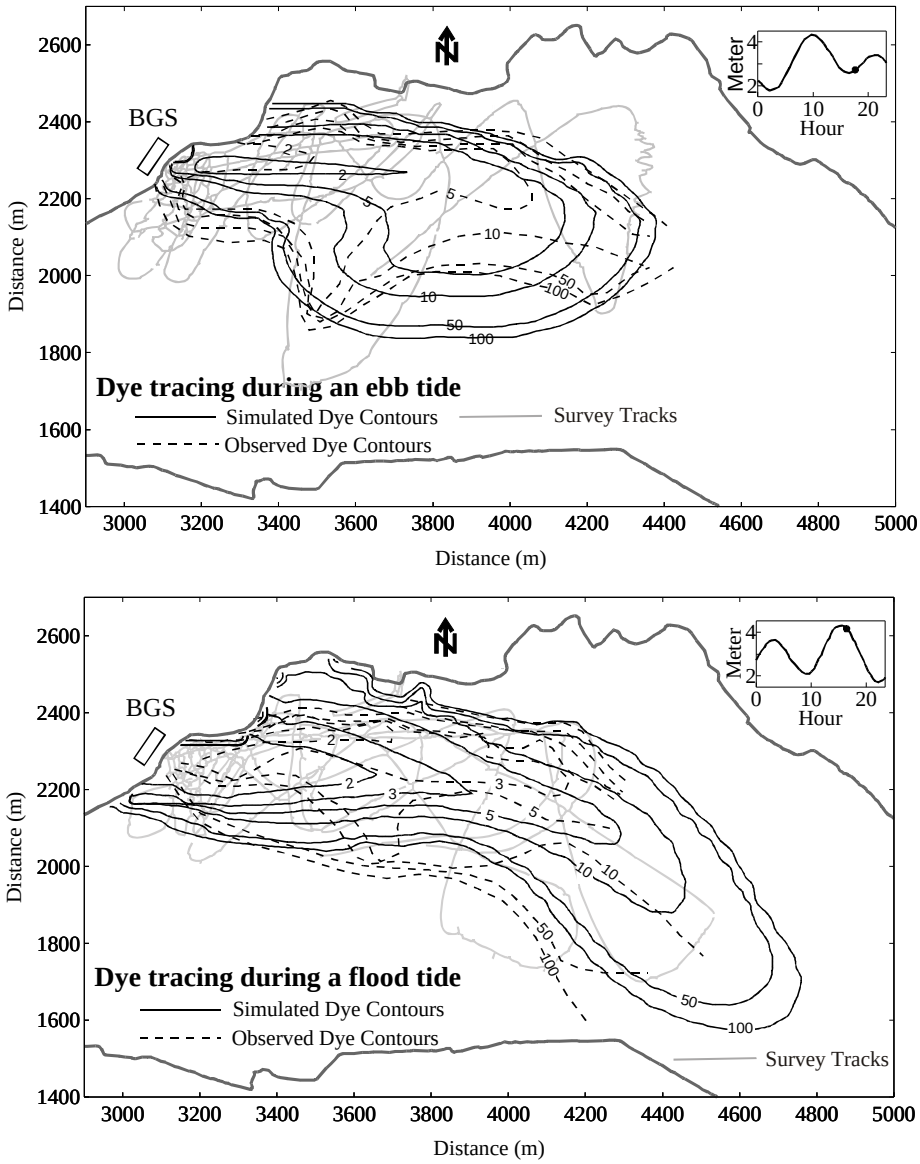

FIGURE 4. Simulated dye dilutions (solid contours) at the end of an ebb tide (upper panel) and the end of a flood tide (lower panel), with comparisons to the dye tracing data (dashed contours). The observed dye contours and survey tracks are from Hodgins and Webb (1991).

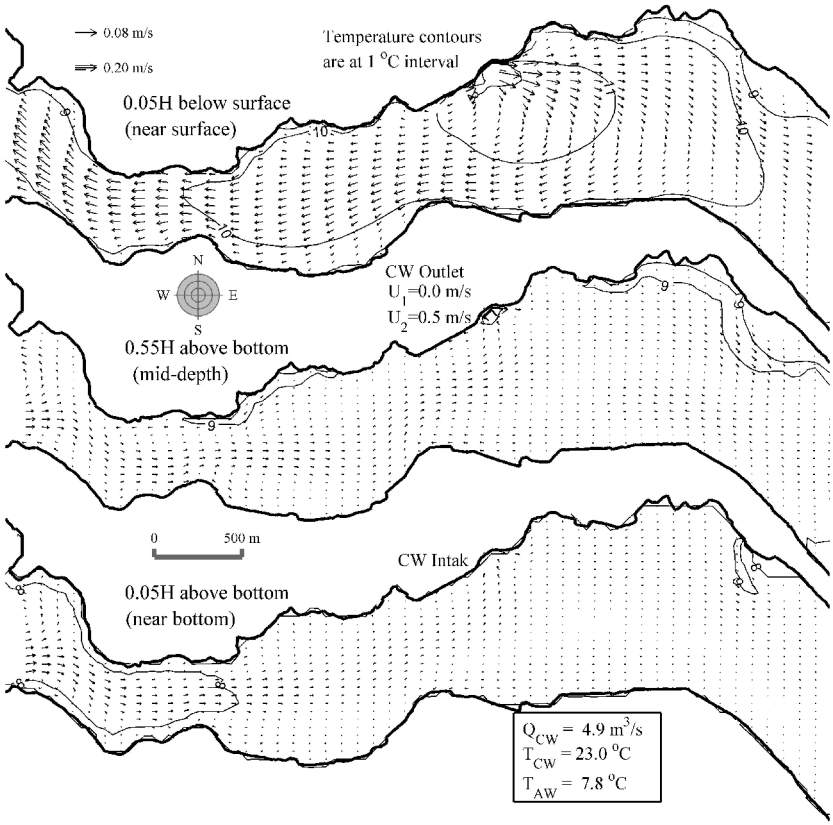

FIGURE 5. Simulated residual currents and tidally-averaged temperatures at near-surface, mid-depth and near-bottom in February, 1998, with U_1 = 0.0 m/s and U_2 = 0.5 m/s.

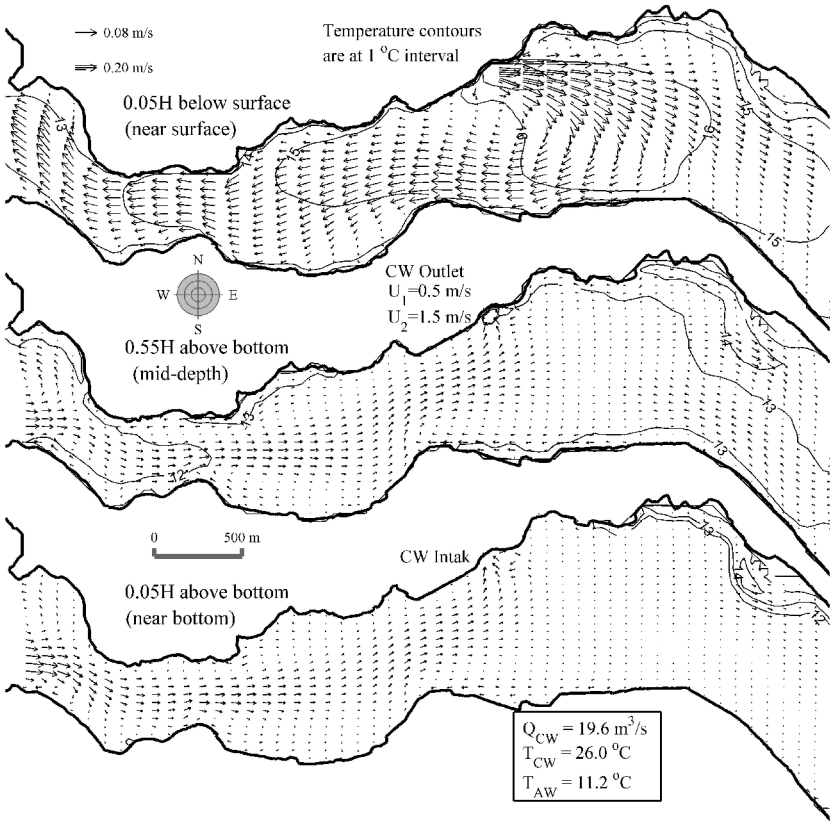

FIGURE 6. Simulated residual currents and tidally-averaged temperatures at near-surface, mid-depth and near-bottom in October, 1998, with U_1 = 0.5 m/s and U_2 = 1.5 m/s.

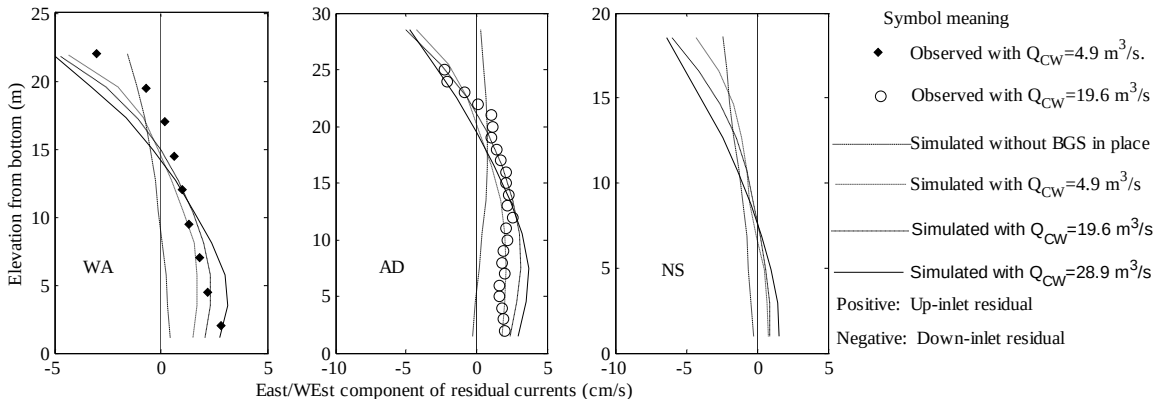

FIGURE 7. Simulated residual profiles at sites WA, AD and NS under different BGS conditions, with comparisons to the observations at WA and AD. Site locations are plotted in Figure 1.